NANOSYSTEMS:
PHYSICS, CHEMISTRY, MATHEMATICS

Original article

Kuchko A.V., Smirnov A.V. *Nanosystems: Phys. Chem. Math.*, 2022, **13** (1), 62–70.
http://nanojournal.ifmo.ru
DOI 10.17586/2220-8054-2022-13-1-62-70

Iterative method of reconstructing the size distribution function of spherical nanoparticles based on the intensity of the small-angle X-ray scattering including the interference contribution to the intensity

Artem V. Kuchko[a], Alexander V. Smirnov[b]

ITMO University, St. Petersburg, Russia

[a]artemkav@gmail.com, [b]smirnav_2@mail.ru

Corresponding author: Artem V. Kuchko, artemkav@gmail.com

PACS 61.10.Eq, 61.43.Gt, 61.46.+w

ABSTRACT It has been shown that for systems of polydisperse spherical particles the interference distortions of the scattering intensity significantly affect the result of reconstructing the particle size distribution when the volume fraction of the scattering substance is higher than 10 %. We have developed an iterative method that reconstructs the size distribution function from the small-angle X-ray scattering intensity with interference distortions. The efficiency of this method is confirmed based on simulated scattering intensities and experimentally measured intensities of samples with a volume fraction of a scattering substance up to 40 %.

KEYWORDS small-angle X-ray scattering, polydisperse nanoparticle system, interference contribution, volume fractions distribution, statistical regularization method, iterative methods

FOR CITATION Kuchko A.V., Smirnov A.V. Iterative method of reconstructing the size distribution function of spherical nanoparticles based on the intensity of the small-angle X-ray scattering including the interference contribution to the intensity. *Nanosystems: Phys. Chem. Math.*, 2022, **13** (1), 62–70.

1. Introduction

Materials composed of particles whose sizes range from 1 to 100 nm are widely used in the production of new materials [1–5]. One method that provides direct information about the size, morphology, and structure of nanoparticles is small-angle X-ray scattering (SAXS) [6]. When it comes to particles of a particular shape, this method makes it possible to determine the particle size distribution [7,8]. One of the significant limitations of the SAXS method is the initial section intensity distortion caused by interference from the individual particles [6, 9].

In most cases, the task of reconstructing a size distribution function (SDF) based on the scattering intensity is resolved without taking into account interference contributions [10–14]. The authors have previously developed a statistical regularization method (SRM) [8] representing the Bayesian approach to reconstructing the volume fraction distribution function (VFDF), which is a variant of SDF. This method is also used for highly sparse systems, since in such systems interference contributions to the scattering intensity are extremely negligible. Sparse systems are those systems whose volume fraction φ of the scattering substance does not exceed several percent. Such systems include, for example, powder suspension in a liquid, or a highly diluted powder component as a constituent of a composite material [15].

Nevertheless, when directly examining powder samples, the volume fraction φ of the scattering substance can represent a significant value. For zirconium dioxide as an example, the density of the powder substance itself equals $\rho_0 \cong 6.0$ g/cm^3 [16], while the bulk density of the powder sample can amount to $\rho \cong (1.2...2.5)$ g/cm^3. In such a sample, the volume fraction $\varphi = \rho/\rho_0$ may range from 20 – 40 %. In this case, disregarding the interference contributions in determining the size distribution, as discussed in Section 2, can lead to significant distortions in the reconstruction of a distribution function.

Speaking of spherical particles, Pederson [17] made what is possibly the only successful attempt to solve the problem of particle size distribution using the SAXS intensity including interparticle interference contributions. The basis of the solution proposed in that work represents a nonlinear least square method for selecting coefficients in the B-spline distribution function expansion. The approach suggested in [17] employs local monodisperse approximation (LMA), which simplifies calculating scattering intensity in comparison to a more precise method [18], based on the Percus–Yevick approach.

Still, LMA poses constraints on the distribution features of scattering inhomogeneities in the system that is being examined. These constraints, as follows from [17], are not critical for the system in which the values of scattering inhomogeneities change in space slowly enough, as can be seen, for instance, in solid solutions. At the same time, though, the LMA conditions are hardly ever met when investigating less ordered systems – powders, for example.

This paper suggests an alternative approach to the task of SDF reconstruction based on the intensity with regard to interference contributions. This approach is based on employing an analytical expression of the intensity of SAXS [18] for the system comprised of spherical particles of different sizes. Such expression can be found in the Percus–Yevick approach. Within the framework of the suggested approach, we propose an iterative procedure that simultaneously reconstructs both the volume fraction distribution function of radii of gyration and the corresponding structure factor.

In Section 2, we evaluate the degree of the distortion of the VFDF – reconstructed disregarding interference contributions – dependent on the φ volume fraction of the scattering substance for the typical model distribution, and we describe the proposed iterative procedure for reconstructing the VFDF based on the SAXS intensity. In Section 3, we explain the necessary preliminary procedure for processing the experimental SAXS curves of powder samples. In Section 4, we present the results of applying the iterative procedure for reconstructing VFDF from SAXS intensities calculated based on the model VFDF for different values of φ. In this section,we also present the results of applying the iterative procedure to the experimental intensities of powders composed of ZrO_2+Y_2O_3 with different component ratios.

2. Theory

2.1. Errors of reconstructing distribution function,disregarding interference distortions of the scattering intensity

Using a model distribution as an example, we shall estimate the error in reconstructing the particle size distribution when the reconstruction procedure disregards interference distortions of the scattering intensity. We have chosen the following form for the volume fraction distribution function as model one:

$$f(R_g) = R_g^{k-1} \frac{e^{-R_g/\theta}}{\theta^k \Gamma(k)}, \tag{1}$$

in which R_g is radius of gyration, $k = 6$, $\theta = 2.5$, and $\Gamma(k)$ is the Euler gamma function. Similar distributions can, for example, be observed using electron microscopy on zirconium dioxide nanopowder obtained under hydrothermal conditions [14, 19, 20]. The distribution (1) coincides with the distribution used in the development of SRM [8].

For a chaotic system of spherical particles with a hard sphere interaction potential and a discrete set of radii, formulae for calculating the intensity $I(q)$ as a function of the scattering vector modulus q for a given value φ are described in [18]. Formulae for calculating the scattering intensity for a continuous SDF, obtained by generalizing from those derived in [18] are given in the Appendix.

For distribution (1), assuming that scattering density of the particle material equals 1, the intensity was calculated for volume fraction values $\varphi = 10^{-6}$, and values of from 0.05 and 0.4 at 0.05 intervals (see the first row of Table 1). Instances of the intensity graphs are given in Fig. 1(a). There is an obvious discrepancy between the scattering intensity curves for low values of a scattering vector, where interference contributions are most notable.

TABLE 1. Relative difference (4) between the reconstructed VFDF f_+ and the actual f for different values of the scattering substance volume fraction φ. Functions f_+ were reconstructed disregarding interference contributions.

φ	10^{-6}	0.05	0.1	0.15	0.2	0.25	0.3	0.35	0.4
$\delta(f, f_+)$, %	0.85	9.6	20	32	44	57	71	84	98

To characterize the contribution of interparticle interference in the scattering intensity, a structure factor is traditionally introduced. It is defined by the following formula:

$$S(q) = \frac{I(q)}{I_0(q)}. \tag{2}$$

Here, $I_0(q)$ denotes scattering intensity obtained by summing the scattering intensities of the individual particles. For spherical particles whose radii of gyration range between $R_{g\,\min}$ and $R_{g\,\max}$, the intensity total is (see [8]):

$$I_0(q) = \int_{R_{g\,\min}}^{R_{g\,\max}} f(R_g)\, \Phi\left(\sqrt{\frac{5}{3}} \cdot q \cdot R_g\right) V\left(\sqrt{\frac{5}{3}} \cdot R_g\right) dR_g. \tag{3}$$

Here, $\Phi(x) = \left(3\dfrac{\sin x - x\cos x}{x^3}\right)^2$ and $V(R) = \dfrac{4}{3}\pi R^3$ is the volume of a sphere of radius R. Fig. 1(b) shows graphs of structure factors that correspond to scattering intensities represented in Fig. 1(a). For the minimal value of $\varphi = 10^{-6}$, the structure factor is practically indistinguishable from 1.

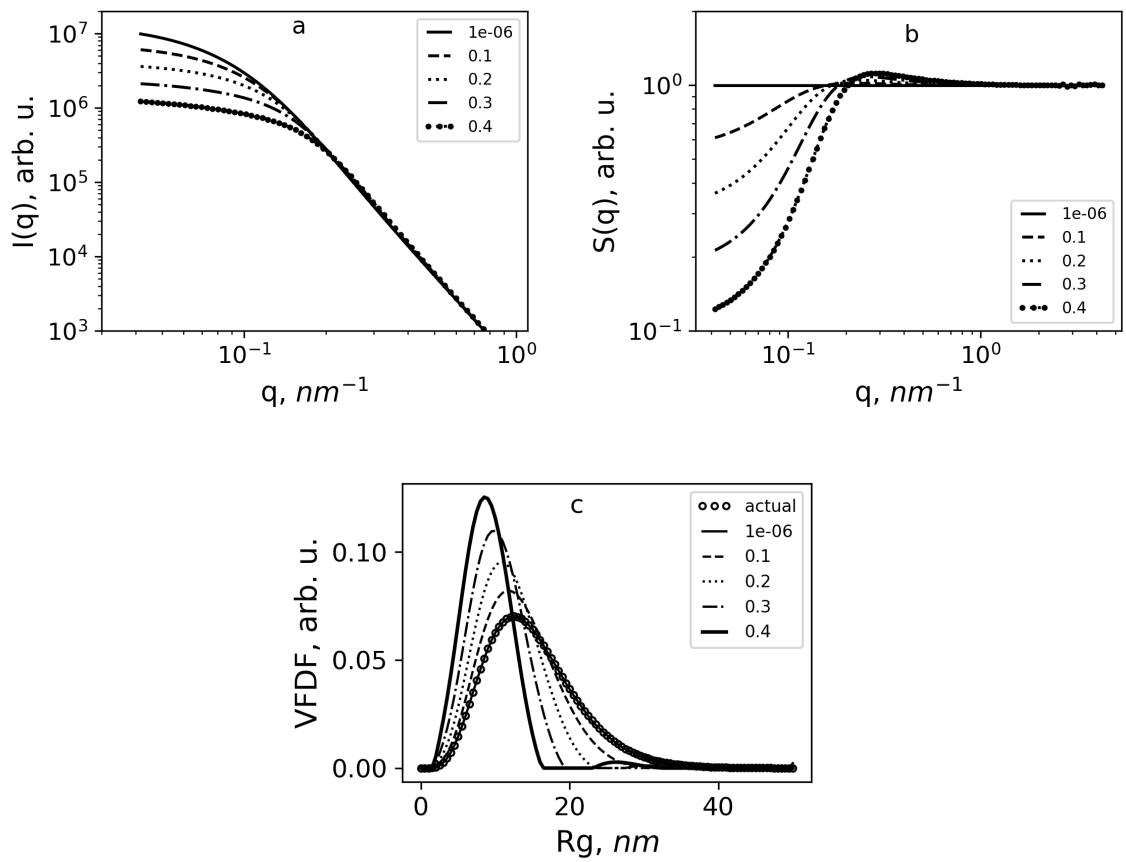

FIG. 1. Analysis results for spherical particle systems with model distribution (1) for different values of φ: a) scattering intensity $I(q)$; b) structure factor $S(q)$; c) actual VFDF and VFDF f_+ reconstructed from intensity $I(q)$, disregarding interference contributions. Values of φ are given in the legend. For easier comparison, the $I(q)$ graphs in Fig. 1(a) were normalized to the same intensity value at the maximum value of the scattering vector modulus

For every scattering intensity value φ without interference contributions, we have used SRM to find the most probable distribution $f_+(R_g)$. The subscript "+" indicates that negative values in the distributions obtained were substituted by zeros.

Normalized functions f_+ reconstructed from the intensity values in Figure 1a are given in Fig. 1(c). This figure clearly shows that the increase in the scattering substance volume fraction leads to considerable distortions of the reconstructed distribution – to the tapering of the distribution support and to the shift of the maximum to the lower radius of gyration values.

For quantitative comparison between the obtained functions f_+ and the actual distribution function f we use the relative difference:

$$\delta(f, f_+) = \frac{\|f - f_+\|}{\|f\|}. \tag{4}$$

Here, $\|\ldots\|$ represents the norm of function set by the following formula:

$$\|f\| = \sqrt{\int_{R_{\min}}^{R_{\max}} \left(f(R_g)\right)^2 dR_g}. \tag{5}$$

Values $\delta(f, f_+)$ for the function f_+ obtained for different values of φ are given in Table 1. It can be seen that already at the value $\varphi \geq 0.1$ the reconstruction error becomes significant – it represents several tens of percent.

For calculations that include interference contributions to the scattering intensity in a polydisperse spherical particle system, we have devised a script in the Python 3.7 programming language, using libraries numpy, scipy, and matplolib. The script is available at [https://gist.github.com/sp_intens_vrija]. As input data, the procedure takes the normalized particle number distribution function for radii, which is reconstructed together with VFDF.

2.2. Iterative method of reconstructing the distribution function including the interference contributions to the scattering intensity

The graphs in Fig. 1(c) show that as the scattering substance volume fraction grows, the reconstructed distribution function f_+ monotonically changes, but at the same time, the support of the function overlaps to a considerable extent with the support of the actual distribution function (1). It is safe to assume that the structure factor calculated based on f_+ will be similar to the structure factor corresponding to the actual function (1), and the initial intensity "corrected" with the inclusion of the structure factor obtained based on f_+ will be similar to the scattering intensity without interference contributions. What follows is the proposed iterative restoring procedure, based on these considerations.

The distribution $f_+^{(1)}$ obtained by SRM from the initial scattering indicatrix $I_{src}(q)$ is the first approximation for the sought distribution function.

The iterative procedure cycle involves the following steps:

(1) Based on the distribution $f_+^{(i)}$ (where i is the index of current iteration) and the given volume fraction φ of scattering substance, we calculate the scattering intensity $I^{(i)}(q)$ with the interference contributions, as well as the one $I_0^{(i)}(q)$ without these contributions.

(2) We calculate the structure factor:

$$S^{(i)}(q) = \frac{I^{(i)}(q)}{I_0^{(i)}(q)}. \tag{6}$$

(3) We calculate the approximate scattering intensity without interference contributions:

$$I_{iter}^{(i)}(q) = \frac{I_{src}(q)}{S^{(i)}(q)}. \tag{7}$$

(4) Based on $I_{iter}^{(i)}(q)$, we calculate $f_+^{(i+1)}$ using SRM.

It should be emphasized that in the third step of each iteration the numerator of the formula (7) is always the initial scattering indicatrix $I_{src}(q)$.

In the Results section, we will show that for the value of $\varphi = 0.4$, solutions $f_+^{(i)}$ "oscillate" around the actual function f_{src}, but without approaching it. This effect is suppressed by introducing the distribution function intermediate averaging in several subsequent steps. Therefore, for $\varphi > 0.3$, we use a modified iterative procedure, in which after several steps we calculate an average distribution function, which is used as an initial one in the subsequent iterations.

Convergence of the iterative procedure is controlled by a decrease in the relative difference $\delta\left(f_+^{(i-1)}, f_+^{(i)}\right)$ between the results of the two consecutive iterations as the number i of the iterations increases.

Cross-platform application SAXSEV 2.1. [21], which employs a Bayesian approach in reconstructing VFDF, was supplemented with a module that launches the recovery of VFDF in the iterative mode. The last version available at https://github.com/artemus-tech/SAXSEV.

3. Preliminary processing of experimental SAXS curves of powder samples

To test the iterative method, we utilized SAXS curves of powder samples composed of ZrO_2+Y_2O_3 synthesized under hydrothermal conditions [22]. These samples had a wide variety of component ratios: the mass fraction of yttrium oxide varied from 3 to 44 %. They were characterized by a significant difference in the average size of nanoparticles.

For these samples (see example in Fig. 2(a)), the shape of experimental SAXS curves differed noticeably from the theoretical one presented in Fig. 1(a). Firstly, for small values of q, and the measured intensity increases sharply as q decreases. This increase is probably due to the presence of agglomerates of large particles in the sample. Secondly, for large values of q, Porod's Law does not apply because of the presence of intraparticle heterogeneities at the atomic level, since the scattering of these heterogeneities makes a permanent contribution to the intensity [23].

These features complicate the direct application of the described iterative procedure, making the preliminary processing of experimental intensities necessary. We shall discuss this processing on the example of the typical scattering intensity (sample with the yttrium mass fraction of 10 %).

To eliminate a constant contribution for large values of q, classical methodology was used [24]. For large values of q, the main non-oscillating contribution to the scattering intensity behaves in this manner:

$$I(q) = A_0 + \frac{A_1}{q^4}. \tag{8}$$

It follows from this formula that the dependence $I \cdot q^4$ vs. q^4 is close to linear, and the coefficient A_0 is the slope of this dependence. After subtracting the obtained value A_0 from the intensity, we obtain the intensity $I'(q) = I(q) - c_0$, which, for the large values of q, behaves like $\sim q^{-4}$ (Porod's Law). The range in which the linear $I \cdot q^4$ vs. q^4 dependence approximation runs lies between the value q_1, at which deviations from the Porod's Law are still not discernible, and the maximum value q_2 (see Fig. 2(a)).

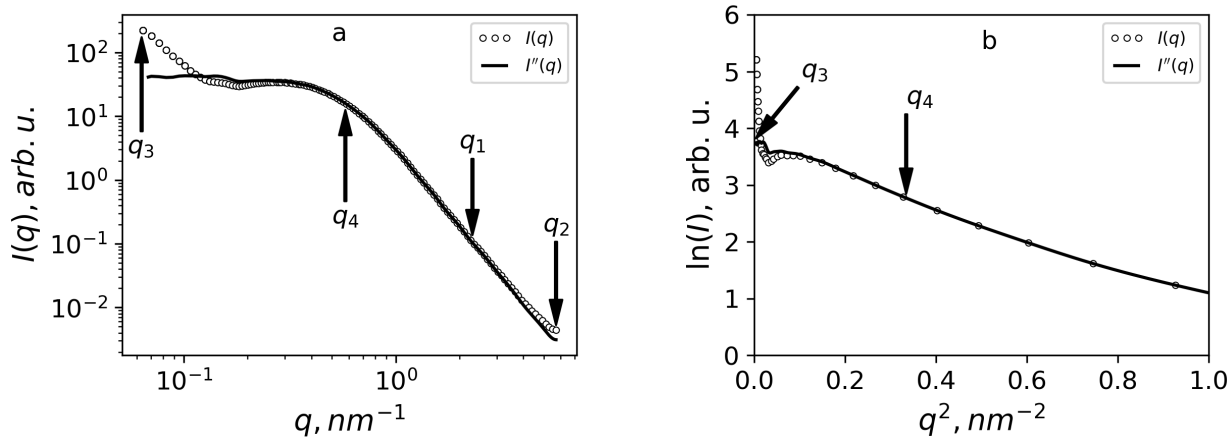

FIG. 2. Experimental intensity $I(q)$ SAXS of the powder sample composed of ZrO_2+Y_2O_3 (mass fraction of yttrium oxide amounts to 10 %) and the intensity $I''(q)$ obtained after preliminary processing: a) Intensities in the whole experimental range; b) Initial section of the graphs $\ln(I)$ vs. q^2. The indicated ranges (q_1, q_2), (q_3, q_4) are used to eliminate contributions of atomic-scale and large-scale inhomogeneities, respectively

In the initial section, intensity $I'(q)$ as well as $I(q)$ rises sharply, and its log-log plot is similar to the linear one. Such behavior gives evidence of a fractal-type distribution of the scattering density in the scale of relatively large sizes corresponding to small values of q. Structure factor for volume fractal looks like this [25]:

$$S_f(q, D, \xi, r_0) = 1 + \frac{D \cdot \Gamma(D-1)}{(qr_0)^D \left[1 + (q\xi)^{-2}\right]^{(D-1)/2}} \sin\left[(D-1)\arctan(q\xi)\right]. \tag{9}$$

On the other hand, when there is no fractal distortion, the scattering intensity logarithm $\ln(I)$ in the initial section (for sufficiently small values of q) is supposed to be a linear function of q^2 [26]. If we denote the intensity without fractal distortion as $I''(q)$, then:

$$\ln(I''(q)) = a + bq^2. \tag{10}$$

Intensity $I'(q)$can be represented as a product of a fractal structure factor (9) and undistorted intensity $I''(q)$: $I'(q) = S_f(q, D, \xi, r_0) \cdot I''(q)$, and its logarithm can be expressed with the formula (10):

$$\ln(I'(q)) = \ln(S_f(q, D, \xi, r_0)) + a + bq^2. \tag{11}$$

To extract $I''(q)$, it is necessary to find optimal parameter values D, ξ, r_0, a, b in the formula (11). These values have been obtained by minimization of the following estimating function:

$$\Delta(D, \xi, r_0, a, b) = \sum_{i=1}^{M} \left[\ln(I'(q_i)) - \left(\ln(SF(q_i, D, \xi, r_0)) + a + bq_i^2\right)\right]^2. \tag{12}$$

Here, the summation is performed on the initial M points in the argument range from the initial value q_3 to q_4, which is an approximate section boundary of the linear $\ln(I)$ dependence of q^2 (see Fig. 2(b)). Using the structure factor (9) with the optimal values for parameters $D^{opt}, \xi^{opt}, r_0^{opt}$, we can finally obtain the undistorted intensity:

$$I''(q) = \frac{I'(q)}{S_f\left(q, D^{opt}, \xi^{opt}, r_0^{opt}\right)}. \tag{13}$$

Figure 2(a) represents the primary experimental intensity $I(q)$ and the reduced intensity $I''(q)$ when the mass fraction of yttrium oxide equals 10 %.

The described preliminary processing procedure was used for all experimental intensities.

4. Results

4.1. Using the iterative procedure for VFDF reconstruction based on the model intensities of SAXS

The iterative procedure described above was tested for VFDF (1) for scattering substance volume fraction $\varphi = 0.1, 0.2, 0.3$, and 0.4. We can see in Fig. 3 for different values of φ the behavior of relative differences in VFDF $\delta\left(f_+^{(i-1)}, f_+^{(i)}\right)$ that were obtained after the $(i-1)$-th and i-th iterations, as well as the relative difference $\delta\left(f_{src}, f_+^{(i)}\right)$ between the actual VFDF and the result of the i-th iteration.

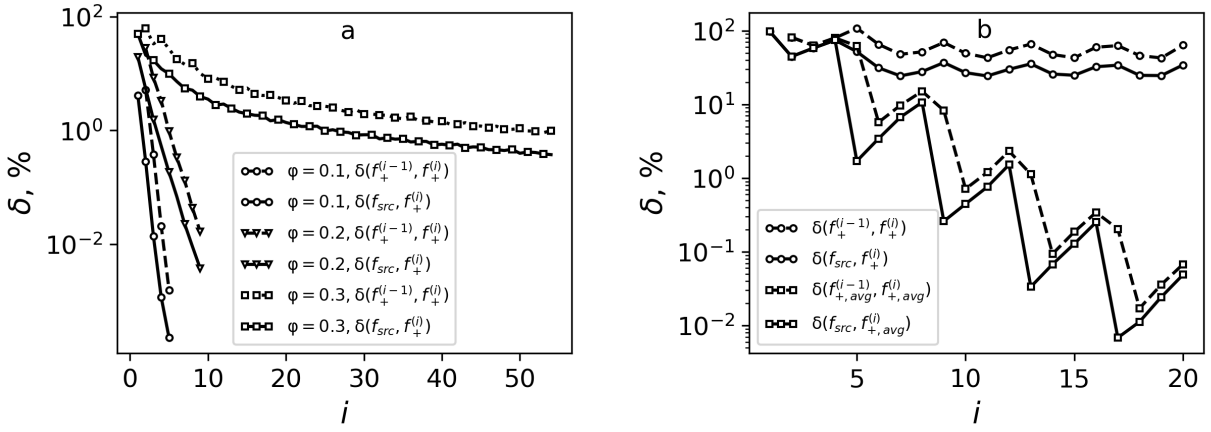

FIG. 3. Dependence of relative VFDF differenceson the number of iterations: a) for $\varphi = 0.1, 0.2, 0.3$ with no intermediate averaging; b) for $\varphi = 0.4$ with no intermediate averaging and with averaging after every fourth iteration following the previous four iterations. VFDFs, obtained using a modified iterative procedure with intermediate averaging, are marked with a subscript "avg"

As it can be seen in Fig. 3(a), for the value $\varphi \leq 0.3$ the iterative procedure converges to the actual distribution function without intermediate averaging. As the number of iterations increases, both relative differences $\delta\left(f_+^{(i-1)}, f_+^{(i)}\right)$ and $\delta\left(f_{src}, f_+^{(i)}\right)$ decrease practically monotonically. If the intermediate averaging is not employed, for the value of $\varphi = 0.4$ (see Fig. 3(b)), as the number of iterations increases, both functions $\delta\left(f_+^{(i-1)}, f_+^{(i)}\right)$ and $\delta\left(f_{src}, f_+^{(i)}\right)$ – oscillate, while their minima do not fall off below 20 %. Intermediate averaging after four consecutive iterations improves the convergence significantly. Fig. 3 also shows that the relative differences between the results of the $(i-1)$-th and the i-th iterations are always larger than the relative difference between the results of the i-th iteration and the actual distribution function.

Table 2 shows the iteration numbers at which the relative differences $\delta\left(f_+^{(i-1)}, f_+^{(i)}\right)$ reach a value less than 1 %; it also shows the corresponding value $\delta\left(f_{src}, f_+^{(i)}\right)$.

TABLE 2. Iteration number i, at which the relative difference $\delta\left(f_+^{(i-1)}, f_+^{(i)}\right)$ diminishes to below 1 %. The last column shows the relative difference between the actual distribution and the result of the i-th iteration.

φ	i	$\delta\left(f_+^{(i-1)}, f_+^{(i)}\right)$, %	$\delta\left(f_{src}, f_+^{(i)}\right)$, %
0.1	3	0.38	0.014
0.2	5	0.96	0.18
0.3	51	0.98	0.42
0.4	3·4+2*	0.094	0.068

*Three complete cycles with intermediate averaging after four iterations + two iterations

4.2. Application of the iterative method for VFDF reconstruction from experimental scattering intensities

Since the volume substance fraction in experimental samples is close to $\varphi = 0.4$, we have used a modified iterative procedure. This procedure results in a considerably rapid convergence: after repeating five cycles consisting of four iterations with intermediate averaging of the results, the relative difference $\delta\left(f_+^{(i-1)}, f_+^{(i)}\right)$ for all samples was less than 0.1 %. The dependence of this relative difference on the number of iterations is represented in Fig. 4(a).

Figure 4(b) shows the normalized reconstructed VFDFs in experimental samples with the scattering substance volume fraction $\varphi = 0.4$ using a modified iterative procedure. Fig. 4(c) facilitates the comparison of the calculated intensities based on VFDFs (Fig. 4(b)) with primary experimental ones. When calculating intensities in Fig. 4(c), parameters c_0, D, ξ, and r_0 calculated in the preliminary processing stage (see Section 3) were utilized.

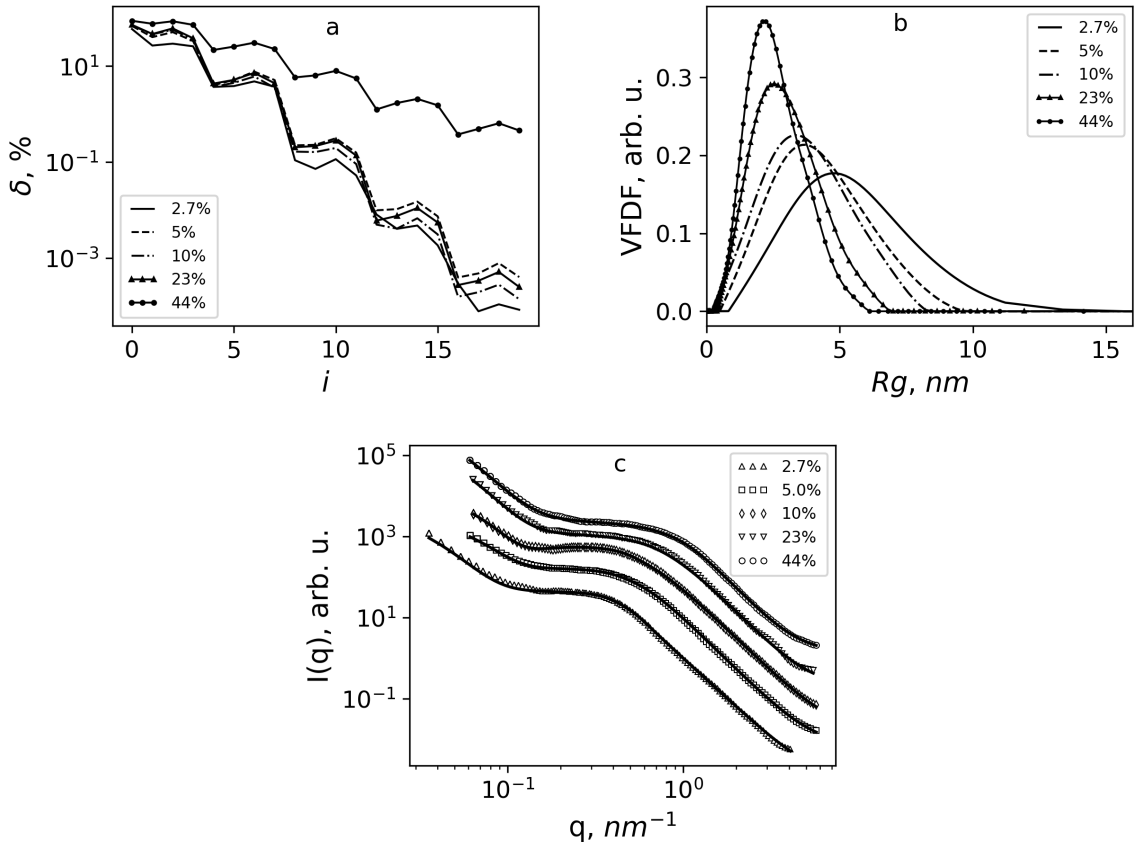

FIG. 4. Results of the application of iterative procedure in relation to SAXS of powder samples composed of ZrO_2+Y_2O_3: a) dependence of the relative difference $\delta\left(f_+^{(i-1)}, f_+^{(i)}\right)$ on the iteration number; b) VFDFs obtained using an iterative procedure; c) comparison of experimental scattering intensities and the intensities calculated on the basis of obtained VFDFs. The legend shows mass fraction of yttrium dioxide in the sample

From Fig. 4(b), it can be seen that as the yttrium oxide mass fraction in the sample goes up, the distribution maximum shifts towards lower values, while the distribution itself becomes narrower. Accordingly, as the yttrium oxide mass fraction increases, the average particle size diminishes to a significant extent, which is in line with prior results [22].

5. Conclusion

This paper proposes an iterative procedure for reconstructing volume fraction distribution function according to radii of gyration in spherical particle systems with a high fraction value φ of scattering substance surface area. The elaborated iterative procedure allows the inclusion of interference contributions into scattering intensity, which, in the case of $\varphi \geq 0.1$, significantly affects the shape of the scattering curve.

The effectiveness of this procedure was verified on the SAXS model curves for typical distribution (1) in the range $\varphi = 0.1...0.4$. The procedure convergence was confirmed by its application to experimental scattering intensities for powder samples of nanoparticles comprised of ZrO_2+Y_2O_3 with a significant difference in yttrium oxide mass fraction.

The iterative procedure suggested in this paper is used for reconstructing the distribution functions of volume fractions in a polydisperse system of particles with a spherical form. However, this procedure is likely to be effective for reconstructing the distributions of particles of other shapes (ellipsoid, cylinder, etc.) as well. The main problem here lies in the manner in which the intensity and structure factor for a polydisperse system of particles of a given form are calculated. The few works that deal with calculating structure factor for non-spherical particles [27, 28] focus solely on monodisperse systems. In line with the development of computer technology, any advancement in the field of investigating polydisperse systems consisting of non-spherical particles will probably be related to a direct simulation of scattering, using methods analogous to the one suggested in [9].

References

[1] Precious-Ayanwale A., Donohu'e-Cornejo A., et al. Review of the synthesis, characterization and application of zirconia mixed metal oxide nanoparticles. *Int. J. of Research – GRANTHAALAYAH*, 2018, **6** (8), P. 136–145.

[2] Larina L.L., Alexeeva O.V., et al. Very wide-bandgap nanostructured metal oxide materials for perovskite solar cells. *Nanosystems: Physics, Chemistry, Mathematics*, 2019, **10** (1), P. 70–74.

[3] Kablov E.N., Stolyarova V.L., et al. Thermodynamics and vaporization of ceramics based on the Y_2O_3–ZrO_2 system studied by KEMS. *J. of Alloys and Compounds*, 2019, **794**, P. 606–614.

[4] Hu C., Sun J., et al. Synthesis of nano zirconium oxide and its application in dentistry. *Nanotechnol Rev.*, 2019, **8** (1), P. 396–404.

[5] Kalinina E.G., Pikalova E.Y. Preparation and properties of stable suspensions of ZrO_2–Y_2O_3 powders with different particle sizes for electrophoretic deposition. *Inorganic Materials*, 2020, **56** (9), P. 941–948.

[6] Guinier A., Fournet G. *Small-angle Scattering of X-rays*. New-York, Wiley, 1955, 268 p.

[7] Agbabiaka A., Wiltfong M., Park C. Small Angle X-Ray Scattering Technique for the Particle Size Distribution of Nonporous Nanoparticles. *J. of Nanoparticles*, 2013, ID 640436, 11 p.

[8] Kuchko A.V., Smirnov A.V. The computation of the nanoparticles volume distribution function and the specific surface area based on the small-angle X-ray scattering indicatrix by the method of the statistical regularization. *Nanosystems: Physics, Chemistry, Mathematics*, 2012, **3** (3), P. 76–91.

[9] Smirnov A.V., Deryabin I.N., Fedorov B.A. Small-angle scattering: the Guinier technique underestimates the size of hard globular particles due to the structure-factor effect. *J. Appl. Cryst.*, 2015, **48**, P. 1089–1093.

[10] Vonk C. On two methods of determination of particle size distribution functions by means of small-angle X-ray scattering. *J. of Applied Crystallography*, 1976, **9** (6), P. 433–440.

[11] Letcher J.H., Schmidt P.W. Small Angle X Ray Scattering Determination of Particle Diameter Distributions in Polydisperse Suspensions of Spherical Particles. *J. Appl. Cryst.*, 1966, **37** (2), P. 649–655.

[12] Yan Y.D., Clarke J.H.R. In-situ determination of particle size distributions in colloids. *Advances in Colloid and Interface Science*, 1989, **29** (3,4), P. 277–318.

[13] Mori Y., Furukawa M., Hayashi T., Nakamura K. Size distribution of gold nanoparticles used by small angle X-ray scattering. *Particulate Science and Technology*, 2006, **24** (1), P. 97–103.

[14] Tyrsted C., Becker J., et al. In-Situ Synchrotron Radiation Study of Formation and Growth of Crystalline $Ce_xZr_{1-x}O_2$ Nanoparticles Synthesized in Supercritical Water. *Chem. Mater.*, 2010, **22**, P. 1814–1820.

[15] Sivtsov E.V., Kalinin A.V., et al. In Situ Preparation of Polymer Nanocomposites Based on Sols of Surface-Modified Detonation Nanodiamonds by Classical and Controlled Radical Polymerization. *Polymer Science, Series B*, 2020, **62** (6), P. 734–749.

[16] Laube J., Gjuqel A., Ottershtedt R. Zirconium oxide and way of its production (Invention RU 2 442 752 C2). Federal service of Russian Federation for intellectual property, 20.02.2012 Bull., 19 p.

[17] Pedersen J.S. Determination of Size Distributions from Small-Angle Scattering Data for Systems with Effective Hard-Sphere Interactions. *J. Appl. Cryst.*, 1994, **27**, P. 595–608.

[18] Vrij A. Mixtures of hard spheres in the Percus-Yevick approximation. Light scattering at finite angles. *J. of Chem. Phys.*, 1979, **71** (8), P. 3267–3270.

[19] Almjasheva O.V., Fedorov B.A., Smirnov A.V., Gusarov V.V. Size, morphology and structure of the particles of zirconia nanopowder obtained under hydrothermal conditions. *Nanosystems: Physics, Chemistry, Mathematics*, 2010, **1** (1), P. 26–36.

[20] Almjasheva O.V., Krasilin A.A., Gusarov V.V. Formation mechanism of core-shell nanocrystals obtained via dehydration of coprecipitated hydroxides at hydrothermal conditions. *Nanosystems: Phys. Chem. Math.*, 2018, **9** (4), P. 568–572.

[21] Kuchko A.V., Smirnov A.V. SAXSEV 2.1 cross-platform application for data analysis of small-angle x-ray scattering from polydisperse systems. *Sci. Tech. J. Inf. Technol. Mech. Opt.*, 2015, **15** (2), P. 267–274.

[22] Shuklina A.I., Smirnov A.V., et al. Structure of nanoparticles in the ZrO_2–Y_2O_3 system, as obtained under hydrothermal conditions. *Nanosystems: Physics, Chemistry, Mathematics*, 2020, **11** (6), P. 729–738.

[23] Ruland W. Small-Angle Scattering of Two-Phase Systems: Determination and Significance of Systematic Deviations from Porod's Law. *J. Appl. Cryst.*, 1971, **4**, P. 70–73.

[24] Feigin L.A., Svergun D.I. *Structure Analysis by Small-Angle X-Ray and Neutron Scattering*. New York, Plenum Press, 1987, 335 p.

[25] Teixeira J. Small-Angle Scattering by Fractal Systems. *J. Appl. Cryst.*, 1988, **21**, P. 781–785.

[26] Guinier A. La diffraction des rayons X aux très petits angles: application à l'étude de phénomènes ultramicroscopiques. *Ann. Phys.*, 1939, **11** (12), P. 161–237.

[27] Hansen S. The structure factor in small-angle scattering and the effect of deviation from spherical symmetry. *J. Appl. Cryst.*, 2011, **44**, P. 265–327.

[28] Hansen S. Monte Carlo estimation of the structure factor for hard bodies in small-angle scattering. *J. Appl. Cryst.*, 2012, **45**, P. 381–388.

Appendix

Formulae for calculating the structure factor for spherical particles with effective hard-sphere interactions.

Let $f(r)$ be a normalized distribution function of the particle amount based on their radii other than zero in the interval $R_{\min}...R_{\max}$, let the particle material unit have scattering density one, and let the scattering substance surface area volume fraction be φ. In that case, scattering intensity per system volume unit equals to

$$I(q) = \frac{6 \cdot \sum\limits_{i=1}^{6} C_i(q)}{\pi \left| F_{11}(q)F_{22}(q) - F_{12}(q)F_{21}(q) \right|^2}, \tag{A1}$$

in which case the following ancillary functions are used:

$$C_1(q) = \left\langle V^2(r)\Phi^2(qr)\right\rangle |T_1(q)|^2; \tag{A2}$$

$$C_2(q) = \left\langle (2r)^6 \Phi^2(qr)\right\rangle |T_2(q)|^2; \tag{A3}$$

$$C_3(q) = 9\left\langle (2r)^4 \Psi^2(qr)\right\rangle |T_3(q)|^2; \tag{A4}$$

$$C_4(q) = 2\left\langle V(r)(2r)^3 \Phi^2(qr)\right\rangle \mathrm{Re}\left(T_1(q)T_2^*(q)\right); \tag{A5}$$

$$C_5 = 6\left\langle V(r)(2r)^2 \Phi(qr)\Psi(qr)\right\rangle \mathrm{Re}\left(T_1(q)T_3^*(q)\right); \tag{A6}$$

$$C_6 = 6\left\langle (2r)^5 \Phi(qr)\Psi(qr)\right\rangle \mathrm{Re}\left(T_2(q)T_3^*(q)\right); \tag{A7}$$

$$T_1(q) = F_{11}(q)F_{22}(q) - F_{12}(q)F_{21}(q); \tag{A8}$$

$$T_2(q) = F_{21}(q)\left\langle 2rV(r)\Phi(qr)e^{iqr}\right\rangle - F_{22}(q)\left\langle V(r)\Phi(qr)e^{iqr}\right\rangle; \tag{A9}$$

$$T_3(q) = F_{12}(q)\left\langle V(r)\Phi(qr)e^{iqr}\right\rangle - F_{11}(q)\left\langle 2rV(r)\Phi(qr)e^{iqr}\right\rangle; \tag{A10}$$

$$F_{11}(q) = 1 - \xi_3 + \left\langle (2r)^3 \Phi(qr)e^{iqr}\right\rangle; \tag{A11}$$

$$F_{12}(q) = \left\langle (2r)^4 \Phi(qr)e^{iqr}\right\rangle; \tag{A12}$$

$$F_{21}(q) = \frac{1}{2}(1-\xi_3)iq - 3\xi_2 + 3\left\langle (2r)^2 \Psi(qr)e^{iqr}\right\rangle; \tag{A13}$$

$$F_{22}(q) = 1 - \xi_3 + 3\left\langle (2r)^3 \Psi(qr)e^{iqr}\right\rangle; \tag{A14}$$

$$\Phi(X) = 3\frac{\sin(X) - X\cos(X)}{(X)^3}; \quad \Psi(X) = \frac{\sin(X)}{X}. \tag{A15}$$

In expressions (A2)–(A15), we use the following notation:

$$V(r) = \frac{4}{3}\pi r^3; \quad \xi_\nu = \left\langle (2r)^\nu \right\rangle. \tag{A16}$$

Let Υ be a mathematical expression. Then $\langle\Upsilon\rangle$ is as follows:

$$\langle\Upsilon\rangle = \frac{\pi}{6}\frac{\varphi}{V_m}\int\limits_{R_{\min}}^{R_{max}} (\Upsilon)\, f(r)dr, \tag{A17}$$

where

$$V_m = \int\limits_{R_{\min}}^{R_{\max}} V(r)f(r)dr. \tag{A18}$$

Formulae (A1)–(A18) represent a generalization in the case of continuous distribution based on the radii of the formulae obtained in [18] for particle systems with discrete sets of radii.

Submitted 15 December 2021; revised 7 January 2021; accepted 8 January 2021

Information about the authors:

Artem V. Kuchko – ITMO University, 49, Kronverkskiy, St. Petersburg, 197101, Russia; ORCID 0000-0003-0971-0810; artemkav@gmail.com

Alexander V. Smirnov – ITMO University, 49, Kronverkskiy, St. Petersburg, 197101, Russia; ORCID 0000-0002-2677-136X; smirnav_2@mail.ru

Conflict of interest: the authors declare no conflict of interest.